Highly accurate simulations and benchmarking of molecule-surface reactions

Tchakoua, T.

5

Constructing Mixed Density Functionals for Describing Dissociative Chemisorption on Metal Surfaces: Basic Principles

This Chapter is based on:

Tchakoua, T.; Jansen, T.; van Nies, Y.; van den Elshout, R.; van Boxmeer, B. A. B.; Poort, S. P.; Ackermans, M. G.; Beltrão, G. S.; Hildebrand, S. A.; Beekman, S. E. J.; van der Drift, T.; Kaart, S.; Šantić, A.; Somers, M. F.; Kroes, G. J. Constructing mixed density functionals for describing dissociative chemisorption on metal surfaces: some basic principles. *J. Phys. Chem. C* **Submitted**

Abstract

We investigate the ability of mixed, parameterized density functionals combining exchange at the generalized gradient approximation (GGA) level with either GGA or non-local correlation to reproduce barrier heights for dissociative chemisorption on metal surfaces. For this, seven expressions of such mixed density functionals are tested on a database consisting of results for 16 systems taken from a recently published slightly larger database called SBH17. Three expressions are derived that exhibit high tunability and use correlation functionals that are either of the GGA form or of two limiting non-local forms also describing the attractive van der Waals interaction in an approximate way. We also find that, for mixed density functionals incorporating GGA correlation, the optimum fraction of repulsive GGA exchange obtained with a specific GGA density functional is correlated with the charge-transfer parameter, which is equal to the difference of the work function of the metal surface and the electron affinity of the molecule.

5.1 Introduction

Transition states formed by the barriers to dissociative chemisorption (DC) can exert a high degree of rate control over the rates of heterogeneously catalyzed reactions proceeding over metal surfaces[1,2], such as ammonia production[3,4] and steam reforming[5]. It is therefore important to describe such barriers accurately. As discussed in several recent papers[6,7] (see also **Chapter 3**), it is not yet possible to use non-empirical present-day electronic structure theory to compute barriers for DC on metal surfaces with guaranteed chemical accuracy (errors ≤ 1 kcal/mol), although the development of an approach based on diffusion Monte-Carlo certainly holds promise in this respect[8]. Instead, success with achieving a chemically accurate description of DC on metals has so far been based on a semi-empirical approach[6,9]. Here, the specific reaction parameter (SRP) approach to density functional theory (DFT) is used to compute a potential energy surface (PES)[9–15] or to construct forces used in direct dynamics calculations[16–19], and an empirical parameter in the functional used is tuned to achieve agreement between calculated and measured DC or "sticking" probabilities, as now documented extensively elsewhere[6].

While the SRP-DFT approach has already been highly successful, it is also important to recognize that there have been some inadequacies in the approach used so far. An important shortcoming has been that the approach to picking an expression for the SRP functional has been rather ad hoc[9–19]. Approaches used so far have been (i) to take a weighted average of two exchange correlation (XC) functionals within the generalized gradient approximation (GGA)[9,10], (ii) to take a weighted average of two exchange (X) functionals within the GGA and to combine the resulting X functional with a GGA correlation (C) functional[20], (iii) as in (ii), but use a non-local C functional[13,14,18,19] also approximately describing the attractive van der Waals interaction[21,22] (see also **Chapter 2**), (iv) to take a GGA exchange functional that was designed to be tunable[23] and to combine it with non-local van der Waals correlation[11,12], and (v) to use meta-GGA functionals either with semi-local correlation[24] or in combination with non-local correlation[15].

The time is now ripe to address some basis issues in SRP functional construction, such as (i) can we use a generic expression of the density functional (DF) in such a way that the DF will usually work, and (ii) might it be possible to pick the expression in such a way that the tuning parameter (the "specific reaction parameter") can be made to correlate with a specific property of the system. Two recent and closely related developments ensure that the time is now right. The first is that a new database of dissociative chemisorption barrier heights has recently become available, which has been called the SBH17 database[7] (see also

Chapter 3). The database holds reference values of barrier heights to DC for 17 systems, in which H_2, N_2, or CH_4 dissociates over a metal surface. For 14 of these systems the barrier height was determined using SRP-DFT, while for 3 systems a more ad-hoc semi-empirical procedure was used to extract a barrier height from a comparison between theory and experiment[7] (see also **Chapter 3**). In a second development[25] it has become clear that the SRP-DFT approach based on GGA exchange functionals has its limits. So far this approach has only been successful for systems in which the charge transfer parameter ΔE_{CT}=WF-EA > 7 eV[25]. Here WF is the work function of the metal and EA is the electron affinity of the molecule. The SBH17 database therefore mostly contains systems for which this condition has been obeyed, which is the case for 16 out of the 17 systems[7]. For systems with $\Delta E_{CT} < 7$ eV the use of even one of the most repulsive GGA X DFs, i.e., RPBE[26], typically leads to underestimated barrier heights[25].

Here we test several mixed DF expressions to see if we can derive one that works for all or most systems in the recently published database[7] we use here. We also test the suggestion implicit in Ref.[25] that the fraction of RPBE exchange needed in a mixed functional correlates with the value of the charge transfer parameter ΔE_{CT} described above. Our Chapter is set up as follows: In Section 5.2, the Method Section, we give a short description of the database we use, which is essentially our previously published database with one system removed from it, in Section 5.2.1. Section 5.2.2 describes the DFs tested and Section 5.2.3 gives computational details. Section 5.3 presents our results, and conclusions are drawn in Section 5.4.

5.2 Methods

5.2.1 The SBH16 database

The DFs described in Section 5.2.2 have been tested on what we here call the SBH16 database, which is the recently described SBH17 database[7] (see also **Chapter 3**) with the H_2 + Pt(211) system removed from it. The reason that we left out the H_2 + Pt(211) system described here is that the results for this system are not that different from those for the H_2 + Pt(111) system also contained in the SBH17 system, so that not so much is to be gained by adding results for the H_2 + Pt(211) system to the results here presented. The SBH17 database holds results for 8 H_2 + metal surface systems (SBH16 for 7 such systems), 2 N_2 + metal surface systems, and 7 CH_4 + metal systems. The reference values of the barrier heights for these systems and the most important geometrical parameters determining the barrier geometry of the molecule relative to the surface are all

presented in table 2 of Ref.[7] (see also table 3.2 of **Chapter 3**). **Chapter 3** also provides the references to the papers in which fuller descriptions of the barrier geometries and of how they were derived may be obtained.

A few details regarding the SBH17 database are important to this Chapter. One is that the barrier heights and geometries are in principle defined best for the 14 out of the 17 systems (13 in SBH16), for which the reference values were obtained with SRP-DFT. Results for three systems (CH_4 + Ni(100), CH_4 + Ru(0001), and N_2 + Ru($10\bar{1}0$)) were obtained with more ad hoc semi-empirical procedures, as discussed in detail in **Chapter 3**. The result that, of the three systems for which on average the largest errors were found with the density functionals tested, two systems were among the systems for which more ad hoc semi-empirical procedures were used (i.e., CH_4 + Ru(0001), and N_2 + Ru($10\bar{1}0$)) is consistent with the lower accuracy anticipated for the ad hoc procedure (the third system for which the DFs tested were least accurate on average was H_2 + Ag(111)). Finally, a useful number characterizing the SBH16 database is the average value of the absolute values of the barrier heights contained in it, which is 0.687 eV (15.9 kcal/mol).

5.2.2 Mixed density functional expressions

The XC part of DFs used as SRP-DFs have typically been taken as mixtures of the X and C components of standard XC DFs. This has the advantage that constraints enforced in constraint-based X and C DFs can also be enforced in SRP-DFs[27]. Based on previous experience, we test the following expressions for the exchange-correlation part of the mixed DFs:

$$E_{\mathrm{XC}}^{SRP\boldsymbol{x}} = \boldsymbol{x}E_{\mathrm{X}}^{RPBE} + (1-\boldsymbol{x})E_{\mathrm{X}}^{PBE} + E_{\mathrm{C}}^{PBE} \tag{5.1}$$

$$E_{\mathrm{XC}}^{SRPsol\boldsymbol{x}} = \boldsymbol{x}E_{\mathrm{X}}^{RPBE} + (1-\boldsymbol{x})E_{\mathrm{X}}^{PBEsol} + E_{\mathrm{C}}^{PBE} \tag{5.2}$$

$$E_{\mathrm{XC}}^{SRP\boldsymbol{x}-vdW1} = \boldsymbol{x}E_{\mathrm{X}}^{RPBE} + (1-\boldsymbol{x})E_{\mathrm{X}}^{PBE} + E_{\mathrm{C}}^{vdW-DF1} \tag{5.3}$$

$$E_{\mathrm{XC}}^{SRP\boldsymbol{x}-vdW2} = \boldsymbol{x}E_{\mathrm{X}}^{RPBE} + (1-\boldsymbol{x})E_{\mathrm{X}}^{PBE} + E_{\mathrm{C}}^{vdW-DF2} \tag{5.4}$$

$$E_{\mathrm{XC}}^{SRPsol\boldsymbol{x}-vdW2} = \boldsymbol{x}E_{\mathrm{X}}^{RPBE} + (1-\boldsymbol{x})E_{\mathrm{X}}^{PBEsol} + E_{\mathrm{C}}^{vdW-DF2} \tag{5.5}$$

and

$$E_{\mathrm{XC}}^{SRP\boldsymbol{x}-vdW1-ext} = E_{\mathrm{XC}}^{SRP\boldsymbol{x}-vdW1}, \quad if \quad \boldsymbol{x} \geq 0. \tag{5.6a}$$

$$E_{\mathrm{XC}}^{SRP\boldsymbol{x}-vdW1-ext} = E_{\mathrm{X}}^{PBE\alpha} + E_{\mathrm{C}}^{vdW-DF1}, \quad if \quad \boldsymbol{x} = (-1+\alpha) < 0. \tag{5.6b}$$

and

$$E_{\rm XC}^{SRP\boldsymbol{x}-vdW2-ext} = E_{\rm XC}^{SRP\boldsymbol{x}-vdW2}, \quad if \quad \boldsymbol{x} \geq 0. \tag{5.7a}$$

$$E_{\rm XC}^{SRP\boldsymbol{x}-vdW2-ext} = E_{\rm X}^{PBE\alpha} + E_{\rm C}^{vdW-DF2}, \quad if \quad \boldsymbol{x} = (-1+\alpha) < 0. \tag{5.7b}$$

The $E_{\rm XC}^{SRP\boldsymbol{x}}$ DF of Eq.5.1 has been used to arrive at a reparameterized SRP DF for H_2 + Cu(111)[20], the original version being a weighted average of the RPBE[26] and PW91[28] DFs[9]. In the limit $\boldsymbol{x} = 0$ the DF defined by Eq.5.1 corresponds to the PBE[29] DF, and in the limit $\boldsymbol{x} = 1$ it corresponds to the RPBE DF (which has the PBE C DF as the correlation part of its exchange-correlation functional[26]). The PBE DF may be seen as a faster and easier-to-evaluate version of PW91[29]. Choosing Eq.5.1 in attempts to derive an SRP DF for a DC-on-metal-surface system is in accordance with conventional wisdom that PBE often under-predicts and RPBE often over-predicts the barrier height for DC on a metal surface[6].

A drawback of using Eq.5.1 is that with PBE the barrier height for DC on a metal surface may also be overestimated in specific cases, even though this DF has a negative mean signed error (MSE) of -58 meV for the SBH17 database[7]. For this database, overestimated (though often not by much) barrier heights were observed for a few weakly activated or non-activated H_2-metal systems (H_2 + Pt(111), Pt(211), and Ru(0001)), for H_2 + Ag(111), and for a few CH_4 + metal surface systems (CH_4 + Ni(100), Pt(211), and Ru(0001)). To avoid this we replaced the X DF of PBE by the X DF of PBEsol[30], which tends to yield lower barriers, this way obtaining the $E_{\rm XC}^{SRP\boldsymbol{x}sol}$ mixed DF of Eq.5.2. It should be noted that for $\boldsymbol{x} = 0$ $E_{\rm XC}^{SRP\boldsymbol{x}sol}$ does not equal the PBEsol functional, which employs the same expression for the C functional as PBE but uses a different value of a coefficient in it to balance the C part of PBEsol against its X part[30]. However, as we will show the use of $E_{\rm XC}^{SRP\boldsymbol{x}sol}$ comes with the advantage that where necessary it yields lower barrier heights for DC on metals than $E_{\rm XC}^{SRP\boldsymbol{x}}$, and thus $E_{\rm XC}^{SRP\boldsymbol{x}sol}$ is more tunable than $E_{\rm XC}^{SRP\boldsymbol{x}}$. Below, we will call the $\boldsymbol{x} = 0$ limit of $E_{\rm XC}^{SRP\boldsymbol{x}sol}$ PBEsolc, to distinguish it from PBEsol.

A drawback of both Eqs.5.1 and 5.2 is that the attractive van der Waals interaction between molecule and surface is not described with a GGA correlation functional, even though this may be necessary for weakly activated DC of H_2 on metals (where the barrier is usually at a fairly large molecule-surface distance so that a proper description of the van der Waals interaction may be important in spite of its weakness[11,12]) or for CH_4 dissociating on a metal surface[18,19]. For this reason we also test the DFs of the forms $E_{\rm XC}^{SRP\boldsymbol{x}-vdW1}$ of Eq.5.3 and

$E_{\rm XC}^{SRP\boldsymbol{x}-vdW2}$ of Eq.5.4, which contain the vdW-DF1 C functional[21] and the vdW-DF2 C functional[22], respectively. The $E_{\rm XC}^{SRP\boldsymbol{x}-vdW1}$ functional has been used successfully to describe supersonic molecular beam experiments on CH_4 + Ni(111)[18], Pt(111)[19], and Pt(211)[19] and on H_2 + Ru(0001)[13]. The $E_{\rm XC}^{SRP\boldsymbol{x}-vdW2}$ functional has been used successfully to describe H_2 + Ru(0001)[13] and Ni(111)[14] (see also **Chapter 2**).

The DFs described by Eqs. 5.3 and 5.4 may have a similar problem as the DF described by Eq.5.1, i.e., that the barrier height is already overestimated with $\boldsymbol{x}$ = 0, including PBE exchange only. For instance, the SRP-DF found for H_2 + Pt(111)[11] and Pt(211)[12] is given by $E_{\rm XC}^{PBE\alpha=0.57,vdW2} = E_{\rm X}^{PBE\alpha=0.57} + E_{\rm C}^{vdW-DF2}$, where $E_{\rm X}^{PBE\alpha=0.57}$ is the inherently tunable PBEα X DF[23], with α = 0.57. As discussed by the developer of the PBEα X functional[23], PBEα=1 corresponds to the PBE functional, while PBEα=0.52 is very similar to the X part of the WC functional[31], which like PBEsol[30] was developed with a view to a better description of the solid state. The $E_{\rm XC}^{SRP\boldsymbol{x}-vdW2}$ with $\boldsymbol{x}$ = 0 (only PBE exchange) overestimates the barrier height for almost all systems in the SBH17 database. For this reason we have also tested the DF $E_{\rm XC}^{SRP\boldsymbol{x}sol-vdW2}$ of Eq.5.5, which for $\boldsymbol{x}$ = 0 consists of PBEsol exchange and the vdW-DF2 correlation functional. In this limit this DF is expected to yield low barriers like $E_{\rm XC}^{PBE\alpha=0.57,vdW2}$.

To increase the tunability of a mixed DF expression like given by Eqs.5.1, 5.3, and 5.4, PBE exchange can be replaced by PBEsol exchange, as done in Eq.5.2 to obtain a better tunable DF than the DF of Eq.5.1, and in Eq.5.5 to obtain a better tunable DF than the DF of Eq.5.4. An alternative already implicitly used in the construction of SRP-DFs is to replace PBE exchange by PBEα exchange with α<1, as done to obtain $E_{\rm XC}^{SRP\boldsymbol{x}-vdW1-ext}$ of Eq.5.6 (which should be more tunable than $E_{\rm XC}^{SRP\boldsymbol{x}-vdW1}$ of Eq.5.3) and to obtain $E_{\rm XC}^{SRP\boldsymbol{x}-vdW2-ext}$ of Eq.5.7 (which should be more tunable than $E_{\rm XC}^{SRP\boldsymbol{x}-vdW2}$ of Eq.5.4). We have not made use of the possibility of the PBEα functional to interpolate between PBE and RPBE exchange, as the PBEα X functional corresponds to the RPBE X functional only in the limit $\alpha \rightarrow \infty$, which is a rather awkward limit to work with, and less preferred to a situation where switching from PBE to RPBE exchange can be performed by switching a parameter continuously from 0 to 1, as can be done in Eqs. 5.1, 5.3, and 5.4.

The DFs of Eqs. 5.1-5.5, 5.6a, and 5.7a have been evaluated for $\boldsymbol{x}$ = 0, $n\Delta\boldsymbol{x}$ with n=1-9, and, and 1.0, modifying $\boldsymbol{x}$ by steps $\Delta\boldsymbol{x}$ equal to 0.1. The DFs of Eqs.5.6b and 5.7b have been evaluated for α=0.57 ($\boldsymbol{x}$ = -0.43), α=0.70 ($\boldsymbol{x}$ = -0.30), and α=0.85 ($\boldsymbol{x}$ = -0.15). For each system the best value of $\boldsymbol{x}$ was defined for the DFs given by Eqs.5.1-5.7 as described in more detail below. If for the

resulting $\boldsymbol{x}$ we have $0.0 \leq \boldsymbol{x} \leq 1.0$ for a DF defined by one of the Eqs.5.1-5.5 the interpolation was successful and the DF expression can be used for the system considered. Similarly, if for the resulting $\boldsymbol{x}$ we have $-0.43 \leq \boldsymbol{x} \leq 1.0$ for a DF defined by one of the Eqs.5.6-5.7 the interpolation was successful and the DF expression can be used for the system considered. Otherwise, extrapolation was used, and the corresponding generic DF was found not to be able to describe the system successfully.

5.2.3 Computational details

The minimum barrier height is computed as

$$E_b = E_{TS} - E_{asym}. \tag{5.8}$$

In Eq.5.8 E_{TS} is the energy of the system (molecule + surface) at the minimum barrier geometry, while E_{asym} is the energy of the system with the molecule in its equilibrium geometry at a distance from the surface such that molecule and surface no longer interact. In the so-called medium algorithm that we use, which is defined and explained in detail in **Chapter 3**, the surface is set up following DFT geometry optimizations of the bulk lattice (to determine the bulk lattice constant(s) with the DF used) and of the metal slab representing the surface (to determine interlayer spacings in the metal surface slab exposed to vacuum according to the DF used). The geometry of the molecule relative to the surface is taken from earlier SRP-DFT calculations as described in **Chapter 3** (see also table 3.2 of that Chapter). In the asymptotic geometry the equilibrium distance of the molecule is likewise computed with the DF tested[7]. A crucial point is that the surface is not allowed to relax with respect to the incoming molecule in the calculation of E_{TS}. A minor difference with **Chapter 3** is that in the present work the geometry optimization of the bulk representing the surface was done using the geometry optimization method implemented in VASP. In the earlier calculations of **Chapter 3**, a parabola was fitted to the energy of the bulk as a function of the lattice constant, and minimization used to establish the bulk lattice constant. The new approach led to small differences in the values of the barrier heights (of 10 meV or less) with respect to the early results when available for the particular DF tested.

All DFT calculations were performed with a user-modified version of the Vienna ab initio simulation package[32–35] (VASP5.4.4). We also used the Atomic Simulation Environment (ASE)[36,37] as a convenient interface package. All calculations using the vdW-DF1 or vdW-DF2 C functionals were done with the algorithm of Román-Pérez and Soler[38] to speed up their evaluation. All other details regarding the calculations (concerning the pseudo-potentials used, the

handling of spin-polarization in systems containing Ni, the number of metal layers in the slab representing the surface, the size of the surface unit cell, etc.) are the same as in **Chapter 3**, to which we refer for these details.

5.3 Results and discussion.

5.3.1 Equilibrium lattice constants computed with mixed density functionals

Equilibrium lattice constants computed with the mixed density functional expressions not incorporating the van der Waals interaction are shown in Table 5.A.1 of the Appendix, stepping through $\boldsymbol{x}$ in SRP$\boldsymbol{x}$ and SRP$\boldsymbol{x}$sol in steps of 0.1 (results for the other mixed DFs not shown). Comparing with zero-point energy corrected experimental values we obtain the usual result that the PBE DF somewhat underestimates and that RPBE overestimates lattice constants[39,40]. The PBEsolc DF (we recall that PBEsolc is the name we use for the DF with PBEsol exchange and PBE correlation) tends to somewhat underestimate the lattice constant. The PBEsol DF would be expected to do rather well for the lattice constant[40] and we suspect that PBEsolc somewhat underperforms as using PBE correlation with PBEsol exchange should lead to a somewhat unbalanced functional[30]. One might of course vary $\boldsymbol{x}$ in the SRP$\boldsymbol{x}$sol DF to obtain the correct lattice constant, but this is not likely to lead to the correct barrier height as GGA DFs yielding good molecule-surface interaction energies tend to overestimate metal lattice constants[30,41].

5.3.2 Performance of limiting forms of the mixed density functionals

To get an impression of how the mixed density functional expressions will perform as generic expressions for fitting SRP functionals, it is a good idea to look at how their limiting forms perform and compare. For this we first consider the limiting forms of the mixed expressions not using van der Waals correlation functionals, i.e., SRP$\boldsymbol{x}$ (Eq.5.1) and SRP$\boldsymbol{x}$sol (Eq.5.2), which are PBE and RPBE, and PBEsolc (we recall that this is the name we use for the DF with PBEsol exchange and PBE correlation) and RPBE. Figure 5.1 shows that for each system in the SBH16 database the barrier height obtained with PBE is lower than that obtained with RPBE, which correlates well with the finding that PBE often underestimates while RPBE often overestimates barrier heights[6]. Also, for each system in the SBH16 database the barrier height obtained with PBEsolc is lower than that obtained with PBE, suggesting that for the purpose of

fitting barrier heights the SRP$\boldsymbol{x}$sol expression will be tunable over a wider range than the SRP$\boldsymbol{x}$ expression. The barrier heights computed with the PBEsolc, PBE, and RPBE functionals may also be found in Table 5.A.2 of the Appendix.

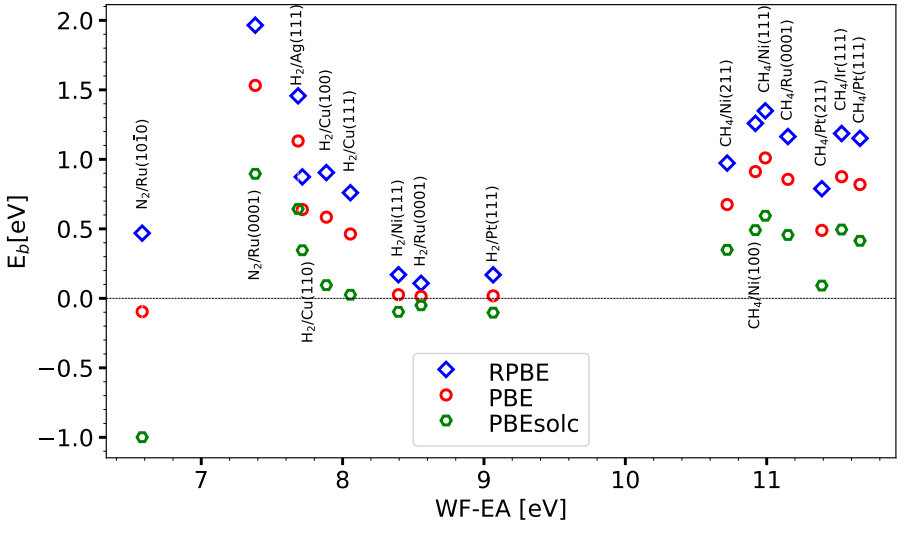

FIGURE 5.1: The barrier heights E$_b$ computed with the PBEsolc, the PBE, and the RPBE DFs are shown as a function of the charge transfer parameter for the 16 systems present in the SBH16 database.

Barrier heights obtained for each system in the SBH16 database with the limiting forms of the SRP$\boldsymbol{x}$ (Eq.5.1), SRP$\boldsymbol{x}$vdW1 (Eq.5.3), and SRP$\boldsymbol{x}$-vdW2 (Eq.5.4) expressions are shown in Fig.5.2 for PBE, PBE-vdW1 and PBE-vdW2, and in Fig.5.3 for RPBE, RPBE-vdW1, and RPBE-vdW2. Whether PBE or PBE-vdW1 yields the lowest barrier height is seen to depend on the value of ΔE_{CT}: for $\Delta E_{CT} \leq 8.055$ eV, PBE yields the lowest barrier height, while for $\Delta E_{CT} \geq 8.395$ eV , PBE-vdW1 yields the lowest barrier height. While this might look odd, one should remember that the correlation part of the vdW-DF1 functional is not just a van der Waals term that is added to an energy expression excluding the attractive dispersion interaction (e.g., the PBE energy). Rather, the vdW-DF1 correlation functional is a different correlation functional than the PBE correlation functional. There is thus no a priori reason that the PBE-vdW1 energy should always be lower than the PBE energy, or vice versa. Furthermore, the barrier obtained with PBE-vdW2 is almost always higher than that obtained with both PBE-vdW1 and PBE (only for H_2 + Ru(0001) is the barrier higher for PBE-vdW1 than for PBE-vdW2). The findings for RPBE, RPBE-vdW1,

and RPBE-vdW2 (Fig.5.3) are analogous to those for PBE, PBE-vdW1, and PBE-vdW2 (Fig.5.2). The barrier heights computed with the PBE, PBE-vdW1, PBE-vdW2 and RPBE functionals may be found in Table 5.A.2 of the Appendix, and the barrier heights computed with the RPBE-vdW1 and RPBE-vdW2 functionals may be found in Table 5.A.3 of the Appendix.

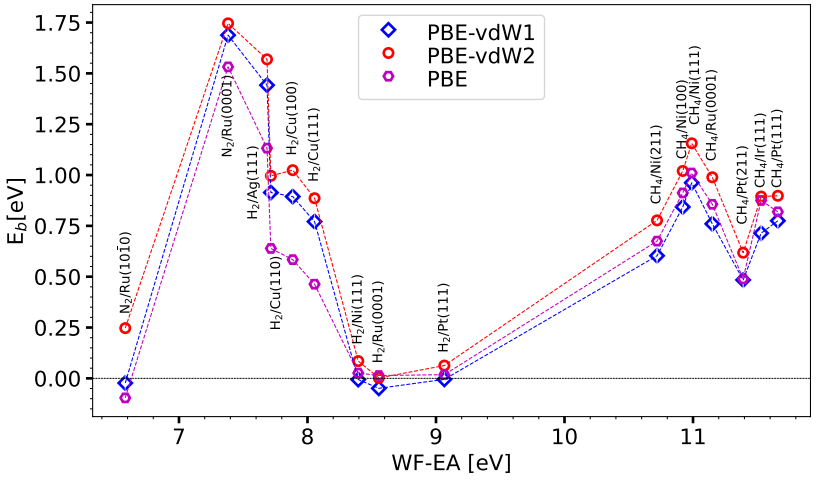

FIGURE 5.2: The barrier heights E_b computed with the PBE, the PBE-vdW1, and the PBE-vdW2 DFs are shown as a function of the charge transfer parameter for the 16 systems present in the SBH16 database.

Barrier heights obtained for each system in the SBH16 database with the lower-limit-forms of the SRP$\boldsymbol{x}$sol (Eq.5.2) and SRP$\boldsymbol{x}$sol-vdW2 (Eq.5.5) expressions are shown in Fig.5.4 for PBEsolc and PBEsol-vdW2. As can be seen the barriers obtained with PBEsolc-vdW2 are always higher than those obtained with PBEsolc, suggesting that the SRP$\boldsymbol{x}$sol-vdW2 DF may be slightly less tunable than the SRP$\boldsymbol{x}$sol DF, which yields very low barriers. The barrier heights computed with the PBEsolc functional may be found in Table 5.A.2 of the Appendix, and the barrier heights computed with the PBEsol-vdW2 functional may be found in Table 5.A.3 of the Appendix.

Finally, barrier heights obtained with the PBEα-vdW1 and PBEα-vdW2 DFs are compared in Fig.5.A.1 of the Appendix for $\alpha = 0.57$, which is the lowest value of α used here. Figure 5.A.1 shows that the PBEα-vdW1 DF consistently yields lower barrier heights than the PBEα-vdW2 DF with $\alpha = 0.57$. This suggests that the PBEα-vdW1 DF is a better tunable mixed DF than the PBEα-vdW2

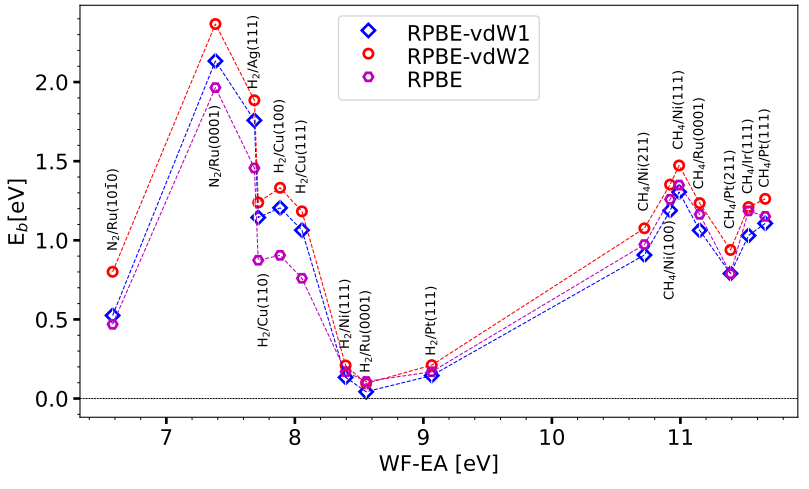

FIGURE 5.3: The barrier heights E_b computed with the RPBE, the RPBE-vdW1, and the RPBE-vdW2 DFs are shown as a function of the charge transfer parameter for the 16 systems present in the SBH16 database.

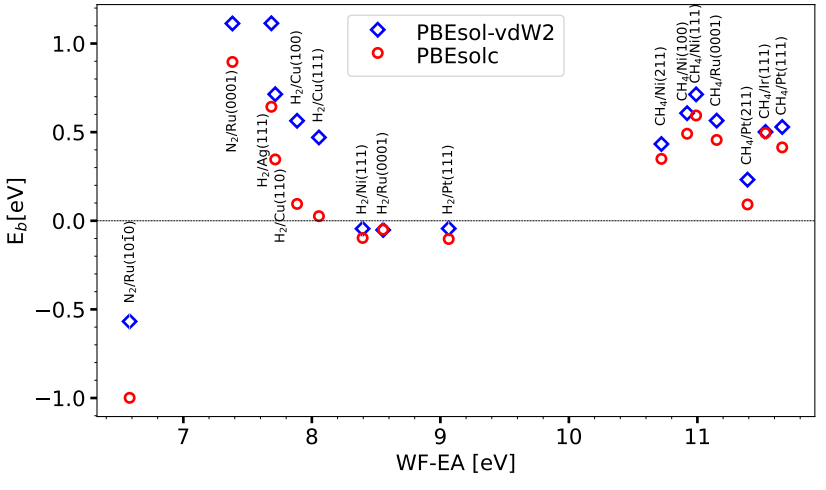

FIGURE 5.4: The barrier heights E_b computed with the PBEsolc and the PBEsol-vdW2 DFs are shown as a function of the charge transfer parameter for the 16 systems present in the SBH16 database.

DF, as the RPBE-vdW1 and RPBE-vdW2 DFs overestimate the barrier height

for each system in the SBH16 database (see the discussion of Table 5.1 below).

Table 5.1 shows mean absolute errors (MAEs) and mean signed errors (MSEs) for the SBH16 database, also comparing to the previous SBH17 results for those DFs that have previously been tested on this database[7]. Here the error for a specific system is defined as the difference between the barrier height computed here and the reference value tabulated in Ref.[7] for that system. As can be seen the MAEs and MSEs computed here for SBH16 differ from previous results known from SBH17 by no more than 10 meV, underscoring the reliability of the results presented here. As previously found, the PBE DF is the best performing DF in terms of the MAE, the MAE being lowest for the PBE DF. Importantly for this study, the DFs serving as upper limits for mixed DFs here (RPBE for SRP$\boldsymbol{x}$ of Eq.5.1 and SRP$\boldsymbol{x}$sol of Eq.5.2, RPBE-vdW1 for SRP$\boldsymbol{x}$-vdW1 of Eq.5.3 and for SRP$\boldsymbol{x}$-vdW1-ext of Eqs.5.6, and RPBE-vdW2 for SRP$\boldsymbol{x}$vdW2 of Eq.5.4, SRP$\boldsymbol{x}$sol-vdW2 of Eq.5.5, and SRP$\boldsymbol{x}$-vdW2-ext of Eq.5.7) all have their MSEs equal to their MAEs, suggesting that these DFs all systematically overestimate the barrier height. This is actually a good quality of a functional that is meant to serve as the upper-limit-form of a mixed DF. The PBEsolc DF, which is the lower-limit-form of the SRP$\boldsymbol{x}$sol DF of Eq.5.2, shows a MSE that is equal to minus its MAE, suggesting that this DF systematically underestimates the barrier height. This is a good quality of a functional that is meant to serve as the lower-limit-form of a mixed DF, and in view of the behavior of the RPBE DF we expect that the SRP$\boldsymbol{x}$sol DF of Eq.5.2 will perform well as a generic expression for reproducing barrier heights by tuning its $\boldsymbol{x}$-parameter. Unfortunately PBE (the lower-limit-form of SRP$\boldsymbol{x}$ of Eq.5.1), PBE-vdW1 (the lower limit of SRP$\boldsymbol{x}$-vdW1 of Eq.5.3), PBE-vdW2 (the lower limit of SRP$\boldsymbol{x}$-vdW2 of Eq.5.4), PBEsol-vdW2 (the lower limit of SRP$\boldsymbol{x}$solvdW2 of Eq.5.5), PBEα57-vdW1 (the lower limit of SRP$\boldsymbol{x}$-vdW1-ext of Eqs.5.6) and PBEα57-vdW2 (the lower limit of SRP$\boldsymbol{x}$-vdW2-ext of Eqs.5.7) all have that their MSE is not equal to minus their MAE, meaning that these DFs do not systematically underestimate the barrier height for the systems in SBH17. Of these DFs, on the basis of the correspondence between their MAE and the negative of their MSE, PBEsol-vdW2 and PBEα57-vdW1 are expected to function best as lower-limit-forms, and consequently the mixed DFs SRP$\boldsymbol{x}$sol-vdW2 and SRP$\boldsymbol{x}$-vdW1-ext are also expected to perform well as tunable mixed DFs.

5.3.3 Performance of mixed density functionals as tunable SRP DFs

Figure 5.5 illustrates how we find the optimal value of $\boldsymbol{x}$ for each mixed DF by showing how this was done for the particular examples of the H_2 + Cu(111) and

TABLE 5.1: Performance of the DFs that represent limiting forms of the mixed density functionals tested on the SBH16 database using the medium algorithm. The mean absolute errors (MAE's) and the mean signed errors (MSE's) are presented in eV for all density functionals investigated here. For the density functionals for which these results are available we also present MAE's and MSE's computed previously for the closely related SBH17 database[7].

Functional	Med Algo			
	MAE	MSE	MAE-SBH17	MSE-SBH17
PBE	0.107	-0.065	0.103	-0.058
RPBE	0.235	0.235	0.228	0.228
PBEsolc	0.458	-0.458	-	-
PBEsol-vdW-DF2	0.269	-0.265	-	-
PBE-vdW-DF1	0.128	-0.020	-	-
PBE-vdW-DF2	0.148	0.117	0.141	0.112
PBEα57-vdW-DF1	0.209	-0.185	-	-
PBEα57-vdW-DF2	0.132	-0.042	0.124	-0.040
RPBE-vdW-DF1	0.278	0.278	-	-
RPBE-vdW-DF2	0.424	0.424	-	-
Average	0.239	0.002	-	-

CH_4 + Pt(111) systems using the mixed DFs SRP$\boldsymbol{x}$ and SRP$\boldsymbol{x}$sol of Eqs.5.1 and 5.2. As Figs.5.5A and 5.5B show the barrier height obtained with a mixed DF typically depends linearly on $\boldsymbol{x}$. This means that the optimal value of $\boldsymbol{x}$ can be found using linear interpolation, i.e., from the point where the linearly interpolated barrier height curves (the sloping red and black lines) intersect the horizontal blue line representing the reference value of the barrier height. If $\boldsymbol{x}$ does not fall between the limits of the mixed DF (0 and 1 for the expressions of Eqs.5.1-5.5, and -0.43 and 1 for Eqs.5.6 and 5.7) a value of $\boldsymbol{x}$ can be found by extrapolation. We have not tested whether the DFs that may be obtained by extrapolation lead to reasonable values of the minimum barrier height; we would not recommend their use. However, the values of $\boldsymbol{x}$ obtained in this way may be used in the calculation of the correlation coefficients discussed in the next Section.

Figures 5.6 and 5.7 show the optimal $\boldsymbol{x}$ coefficients computed for the SRP$\boldsymbol{x}$ and SRP$\boldsymbol{x}$sol DFs of Eqs. 5.1 and 5.2, respectively, as a function of ΔE_{CT}. These coefficients are also listed for each DF in Table 5.A.4. Figure 5.6 shows that obtaining the optimum value of $\boldsymbol{x}$ for the SRP$\boldsymbol{x}$ DF required extrapolation to negative values for several H_2-metal surface and CH_4-metal surface systems. The use of this mixed DF is therefore not guaranteed to yield a useful SRP DF for systems like the ones investigated here. From the point of view of tunability the opposite is true for the SRP$\boldsymbol{x}$sol DF, for which we obtained a value of $\boldsymbol{x}$ falling between 0 and 1 for all systems in the SBH16 database (see Figs.5.6-5.7).

Figure 5.8 shows the optimal $\boldsymbol{x}$ coefficients computed for the SRP$\boldsymbol{x}$sol-vdW2 DF of Eq.5.5 as a function of ΔE_{CT}. These coefficients are also listed for this

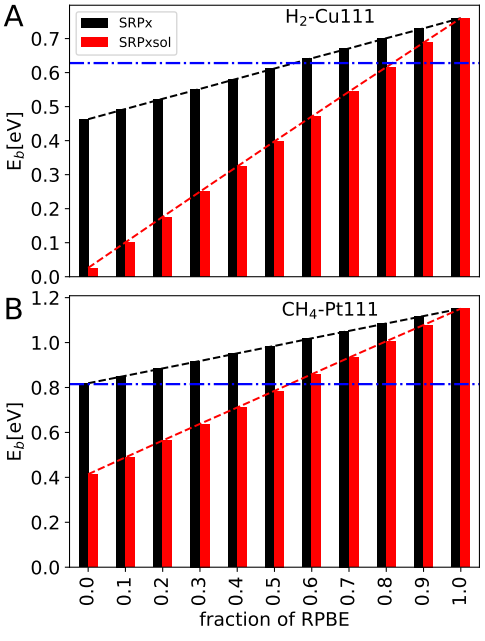

FIGURE 5.5: The barrier heights computed with the SRP$\boldsymbol{x}$ DF (black bars) and the SRP$\boldsymbol{x}$sol DF (red bars) is shown as a function of the fraction of RPBE exchange $\boldsymbol{x}$, (A) for H_2 + Cu(111) (upper panel) and (B) CH_4 + Pt(111) (lower panel). Blue horizontal lines indicate the reference value of the barrier height for these systems[7]. The black and red dashed lines linearly interpolate the barrier height as a function of $\boldsymbol{x}$ for the SRP$\boldsymbol{x}$ and the SRP$\boldsymbol{x}$sol DFs, respectively. The optimal value of $\boldsymbol{x}$ is equal to the value of $\boldsymbol{x}$ for which these lines intersect the blue lines.

DF in Table 5.A.5. Figure 5.8 shows that obtaining the optimum value of $\boldsymbol{x}$ for the SRP$\boldsymbol{x}$sol-vdW2 DF only required extrapolation to a negative value for H_2 + Ag(111). This system was classified as problematic in the SBH17 study, with all DFs tested there yielding large MAEs for this system[7]. While we conclude that the use of this mixed DF is not guaranteed to yield a useful SRP DF for systems like the ones investigated here, we find that it performs rather well, and that it can probably be used if a SRP DF is desired with vdW-DF2 correlation in it. Note that, when coupled to their original partner exchange functionals[21,22], the vdW-DF2 functional[22] yields a better description of the S22 database binding energies of gas phase dimers (MAE of 22 meV)[22] than the vdW-DF1 functional[22] (MAE of 41 meV)[21]. However, the vdW-DF1 functional[21] generally yields a better description of bulk solids[42] than the vdW-DF2 functional[22].

Figure 5.9 shows the optimal $\boldsymbol{x}$ coefficients computed for the SRP$\boldsymbol{x}$vdW1-ext DF of Eq.5.6 as a function of ΔE_{CT}. These coefficients are also listed in

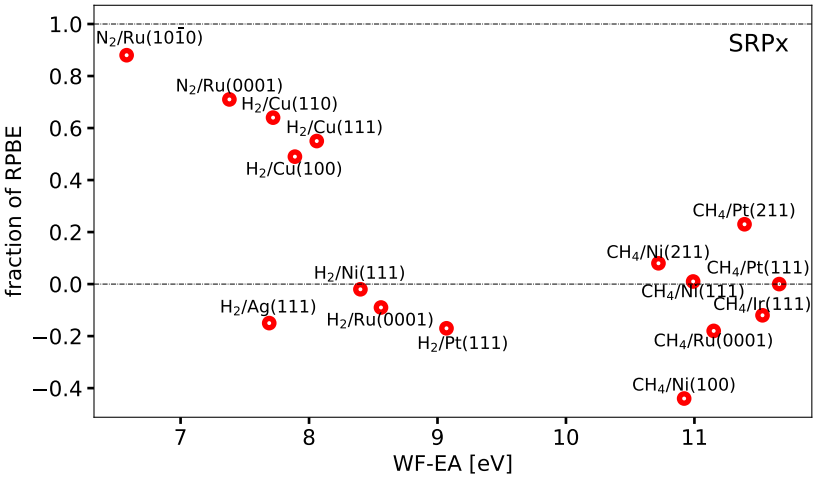

FIGURE 5.6: The optimum fraction of RPBE exchange $\boldsymbol{x}$ is shown as a function of ΔE_{CT} for the SRP$\boldsymbol{x}$ DF (Eq.5.1). Values falling between the two horizontal dot-dashed black lines could be obtained by the interpolation procedure illustrated in Figure 5.5.

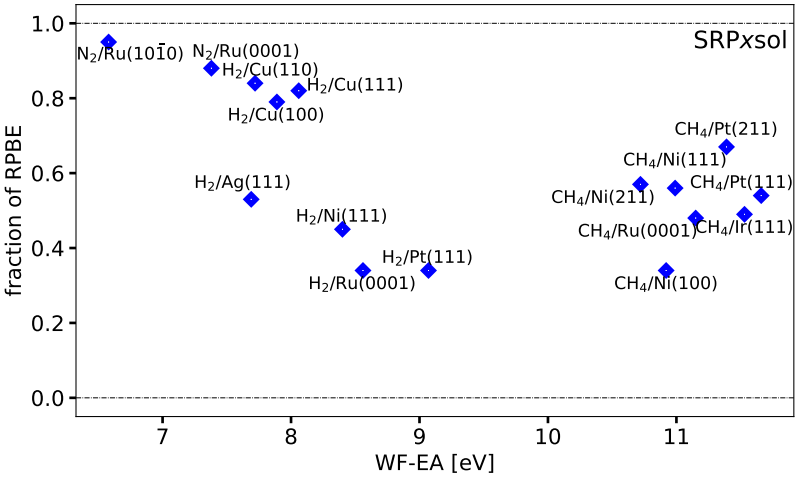

FIGURE 5.7: The optimum fraction of RPBE exchange $\boldsymbol{x}$ is shown as a function of ΔE_{CT} for the SRP$\boldsymbol{x}$sol DF (Eq.5.2). Values falling between the two horizontal dot-dashed black lines could be obtained by the interpolation procedure illustrated in Figure 5.5.

Table 5.A.5. Figure 5.9 shows that obtaining the optimum value of $\boldsymbol{x}$ for the SRP$\boldsymbol{x}$-vdW1-ext DF only required extrapolation to a negative value for H_2 + Cu(110) and H_2 + Ag(111). The latter system was classified as problematic in the SBH17 study, with all DFs tested there yielding large MAEs for this system[7]. The use of the SRP$\boldsymbol{x}$-vdW1-ext DF mixed DF is not guaranteed to yield a useful SRP DF for systems like the ones investigated here, but we find that it performs rather well just like SRP$\boldsymbol{x}$sol-vdW-DF2, and the SRP$\boldsymbol{x}$-vdW1-ext can be used if a SRP-DF is desired with vdW-DF1 correlation in it. As noted above, when partnered with their original exchange functionals vdW-DF1 yields better descriptions of bulk solids, while vdW-DF2 tends to be better for binding energies of gas phase dimers.

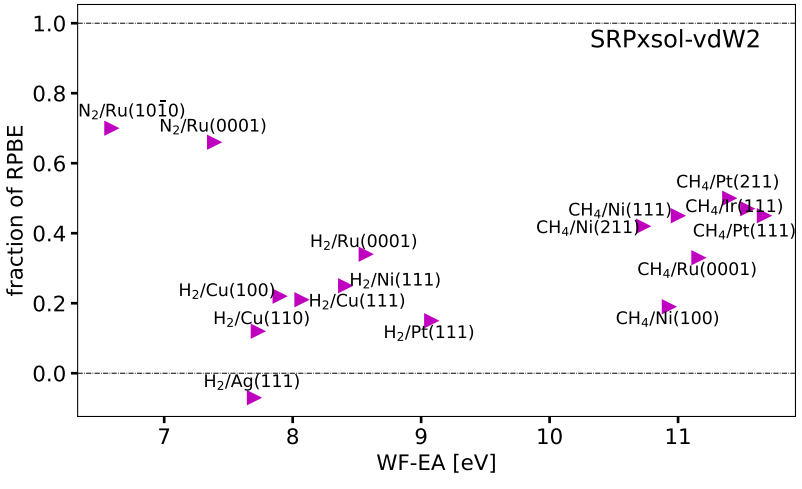

FIGURE 5.8: The optimum fraction of RPBE exchange $\boldsymbol{x}$ is shown as a function of ΔE_{CT} for the SRP$\boldsymbol{x}$sol-vdW2 DF (Eq.5.5). Values falling between the two horizontal dot-dashed black lines could be obtained by the interpolation procedure illustrated in Figure 5.5.

Figures 5.A.2, 5.A.3, and 5.A.4 show the optimal $\boldsymbol{x}$ coefficients computed for the SRP$\boldsymbol{x}$-vdW1, SRP$\boldsymbol{x}$-vdW2, and SRP$\boldsymbol{x}$-vdW2-ext DFs of Eqs. 5.3, 5.4, and 5.7, respectively, as a function of ΔE_{CT}. These coefficients are also listed for each DF in Tables 5.A.4 and 5.A.5. Figures 5.A.2-5.A.4 show that obtaining the optimum value of $\boldsymbol{x}$ for these three mixed DFs required extrapolation to negative values for several H_2-metal surface and in most cases also for several CH_4-metal surface systems, with SRP$\boldsymbol{x}$-vdW2 performing particularly poorly. The above suggests that these three mixed DFs, and especially SRP$\boldsymbol{x}$-vdW2,

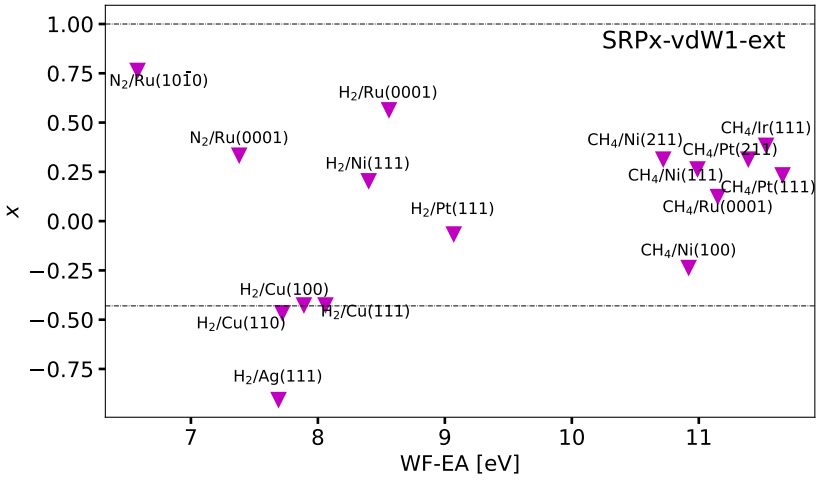

FIGURE 5.9: The optimum mixing parameter $\boldsymbol{x}$ is shown as a function of ΔE_{CT} for the SRP$\boldsymbol{x}$-vdW1-ext DF (Eq.5.6). Values falling between the two horizontal dot-dashed black lines could be obtained by the interpolation procedure illustrated in Figure 5.5.

should perhaps not be the first choice for deriving a new SRP-DF for a system like the ones present in the SBH16 database.

5.3.4 Correlation of the mixing parameter with the charge transfer parameter

Table 5.2 shows correlation coefficients (or Pearson product-moment correlation coefficients)[43] r_{xy} describing the correlation between the charge transfer parameter taken as independent variable and the mixing coefficient $\boldsymbol{x}$ taken as dependent variable, for the seven mixed DFs tested here. Including all systems, the r_{xy} are clearly negative for the SRP$\boldsymbol{x}$ and the SRP$\boldsymbol{x}$sol DFs. The same is true for these DFs if only the H_2-metal systems are considered, and for these systems the r_{xy} values get close to the value of -1 indicating a nearly perfect linear relationship if the H_2 + Ag(111) system, for which the reference barrier height is somewhat suspect, is not considered. For CH_4 metal systems the values of r_{xy} only take on negative values if the CH_4 + Ru(0001) and Ni(100) systems, for which the reference barrier heights are also somewhat suspect, are not considered, and these values are small in absolute value.

The finding of negative correlation coefficients as observed here for the SRP$\boldsymbol{x}$ and SRP$\boldsymbol{x}$sol DFs is what we expected to see, for several reasons. First of all, the MAE of the RPBE DF was previously found to increase from 88 to 167 to 336

TABLE 5.2: Correlation coefficients computed for the dependence of the optimum fraction of RPBE exchange x on the charge transfer parameter for the mixed DFs tested. Computed correlation coefficients are provided for the 7 H_2-metal surface systems present in the SBH16 database, the 6 H_2-metal surface systems obtained once H_2 + Ag(111) is removed, the 7 CH_4-metal surface systems in the SBH16 database, the 5 CH_4-metal surface systems that remain after CH_4 + Ru(0001) and Ni(100) are removed, the 16 systems (All-16) present in the SBH16 database, and the 12 systems (All-12) that remain after the 3 systems already mentioned and N_2 + Ru($10\bar{1}0$) are removed.

type SRP	All-16	All-12	7 H_2-metal	6 H_2-metal	7 CH_4-metal	5 CH_4-metal
SRPx	-0.648	-0.617	-0.584	-0.927	0.211	-0.239
SRP$x$sol	-0.543	-0.409	-0.761	-0.91	0.228	-0.174
SRPx-vdW-DF1	0.264	0.528	0.752	0.684	0.362	0.003
SRPx-vdW-DF2	0.205	0.483	0.751	0.695	0.500	0.801
SRP$x$sol-vdW-DF2	0.147	0.447	0.473	0.209	0.483	0.609
SRPx-vdW-DF1-ext	0.236	0.521	0.716	0.627	0.361	0.003
SRPx-vdW-DF2-ext	0.148	0.423	0.741	0.671	0.420	0.428

meV going from N_2-metal systems to H_2-metal systems to CH_4-metal systems[7], respectively, i.e., going from small values of the charge transfer parameter to large values (see e.g. Table 5.A.2 and Fig.5.6 for how the charge transfer parameter varies with the type of system). The opposite is true for the PBE DF, where the MAE was found to decrease from 409 to 80 to 45 meV going from N_2-metal systems to H_2-metal systems to CH_4-metal systems[7], respectively. Second, tests on several systems suggest that for systems characterized by charge transfer parameters less than 7 eV even RPBE exchange is not repulsive enough to avoid underestimating the barrier height[25]. However, it is also clear that when all three types of systems are considered the correlation is not that strong, suggesting that when a mixed functional with a fraction of PBE correlation is used the optimum mixing coefficient also depends on other properties of the system than the charge transfer parameter. In this context we note that r_{xy} for all systems decreases in absolute value if the four systems with suspect reference values (N_2 + Ru($10\bar{1}0$), CH_4 + Ru(0001), CH_4 + Ni(100), and H_2 + Ag(111))[7] are excluded from the SBH16 database (see Table 5.2), which would not be expected if $\boldsymbol{x}$ would only depend on the charge transfer parameter and the relationship would be linear.

The computed values of the correlation coefficients for the DFs incorporating van der Waals correlation are rather different from the values calculated for SRP$\boldsymbol{x}$ and SRP$\boldsymbol{x}$sol, which incorporate PBE correlation. Restricting ourselves to the mixed DFs that exhibit high tunability, i.e., SRP$\boldsymbol{x}$sol-vdW2 and SRP$\boldsymbol{x}$-vdW1-ext, we see that the former one only exhibits positive correlation coefficients, and that the latter one exhibits correlation coefficients that are either positive or close to zero. The reason for the different values of the correlation coefficients of SRP$\boldsymbol{x}$ and SRP$\boldsymbol{x}$sol on the one hand (mostly negative) and the other DFs incorporating van der Waals correlation on the other hand (mostly positive) are not clear at this stage; the difference is rather puzzling.

5.4 Conclusions and outlook.

We have investigated the tunability of several expressions for mixed density functionals, in which a mixing parameter $\boldsymbol{x}$ can be tuned to enable the mixed DF to reproduce the reference value of the barrier height to dissociative chemisorption of a molecule on a metal surface. The mixed functionals are tested on the barriers collected in the database we call SBH16, which is equal to the previous SBH17 database in **chapter 3** with the H_2 + Pt(211) system removed from it.

Increasing the fraction of RPBE exchange incorporated in the mixed DFs leads to higher barriers. All mixed DFs tested are well tunable towards higher barriers, as their limiting forms (RPBE, RPBE-vdW1, and RPBE-vdW2) all systematically overestimate the barrier height for the systems in the SBH16

database. It turns out that the biggest challenge to finding a perfectly tunable mixed DF for describing the SBH16 database is to obtain a mixed DF expression with a good lower-energy form, which consistently underestimates barrier heights for systems like the ones present in SBH16. This goal is fully met with the mixed SRP$\boldsymbol{x}$sol DF that uses PBE correlation and a mixture of PBEsol and RPBE exchange. The mixed SRP$\boldsymbol{x}$sol-vdW2 DF could describe the minimum barrier height of 15 of the 16 systems using vdW-DF2 correlation, while the mixed SRP$\boldsymbol{x}$-vdW1 DF could do so for 14 of the 16 systems using vdW-DF1 correlation. Being able to use mixed DFs with different correlation functionals may be important to obtaining a SRP DF for a particular system because reproducing the minimum barrier height is a necessary, but not a sufficient condition for reproducing measured sticking (or dissociative chemisorption) probabilities, as now used for validating SRP functionals and barrier heights: It is also necessary to provide a description of how the barrier height varies when the molecule's impact site on the surface and its orientation relative to the surface is changed, and this variation may depend strongly on the correlation functional used[6,13,27].

We also tested whether and how the mixing coefficient of the mixed DFs is correlated with the charge transfer parameter describing the system, i.e., the difference between the work function of the metal surface and the electron affinity of the molecule. The answer depends on which mixed DF is used. For the SRP$\boldsymbol{x}$ and SRP$\boldsymbol{x}$sol DFs, which both use PBE correlation, we found that the optimum fraction of RPBE exchange decreases with the charge transfer parameter, as could be expected on the basis of earlier results. However, the opposite relationship and weaker correlation was found for the mixed DFs using vdW-DF1 or vdW-DF2 correlation. The reason for this difference is not clear.

The results presented here point to several new lines of research. First of all the results underscore the need to obtain better reference values for the H_2 + Ag(111), CH_4 + Ru(0001), and CH_4 + Ni(100) systems. For all mixed DFs the optimized mixing coefficients for these systems appear as outliers when plotted as a function of the charge transfer parameter, and removing these systems from the database leads to correlation coefficients with an increased absolute value for the mixed SRP$\boldsymbol{x}$ and SRP$\boldsymbol{x}$sol DFs for the H_2-metal surface and the CH_4-metal surface systems.

A small improvement over using the SRP$\boldsymbol{x}$sol mixed DF could be to use a DF that simply mixes the RPBE and the PBEsol exchange-correlation functionals. This would avoid the use of an exchange correlation functional with unbalanced exchange and correlation at the lower $\boldsymbol{x}$=0 end of the spectrum, i.e., PBEsolc.

When it comes to designing mixed functionals incorporating vdW-DF1 or vdW-DF2 correlation, another idea worth testing might be to investigate mixtures of weakly repulsive GGA exchange DFs that are appropriate matches for the vdW1

and vdW2 correlation functionals with the rather repulsive[44] exchange functionals combined with these C functionals in the original vdW-DF1[21] and vdW-DF2[22] DFs. Examples of such exchange functionals have been incorporated in the C09[45] and CX[46] vdW functionals, and other exchange functionals mentioned in Ref.[44]. Another idea would be to explore mixtures of repulsive meta-GGA DFs (such as MS-B86bl[24]) and attractive meta-GGA DFs (such as SCAN[47]) that tend to overestimate respectively underestimate barriers to dissociative chemisorption of molecules on metals[7]. It would also be of interest to investigate the performance of mixtures of, or parameterized forms of screened hybrid functionals such as HSE06[48] and screened hybrid functionals incorporating van der Waals correlation[44,49]. However, it might be most productive to test such hybrid functionals once a database becomes available that also incorporates good reference values of barrier heights for systems characterized by charge transfer parameters < 7 eV, such as O_2 + Ag(111)[25] and HCl + Au(111)[50]. Such systems presently defy an accurate description based on DFs incorporating GGA exchange[25,50,51].

5.A Appendix Tables and Figures

TABLE 5.A.1: Measured zero-point-energy-corrected and computed equilibrium lattice constants a of the fcc metals Ag, Cu, Ir, Ni, and Pt, and a and c of the hcp metal Ru are presented. The computed values have been calculated with the SRP$\boldsymbol{x}$ and SRP$\boldsymbol{x}$sol DFs varying $\boldsymbol{x}$ by steps $\Delta\boldsymbol{x}$ of 0.1.

Metal	Ag	Cu	Ir	Ni	Pt	Ru	
	a	a	a	a	a	a	c
Experimental	4.062[52]	3.597[52]	3.831[52]	3.499[52]	3.912[52]	2.703[53]	4.274[53]
			SRP$\boldsymbol{x}$				
PBE	4.147	3.635	3.873	3.518	3.968	2.721	4.293
$\boldsymbol{x}$=0.1	4.153	3.639	3.874	3.521	3.970	2.722	4.295
$\boldsymbol{x}$=0.2	4.159	3.644	3.875	3.524	3.972	2.723	4.297
$\boldsymbol{x}$=0.3	4.165	3.648	3.877	3.528	3.974	2.725	4.299
$\boldsymbol{x}$=0.4	4.172	3.652	3.878	3.531	3.976	2.726	4.301
$\boldsymbol{x}$=0.5	4.178	3.657	3.880	3.535	3.979	2.727	4.303
$\boldsymbol{x}$=0.6	4.185	3.661	3.882	3.539	3.981	2.728	4.305
$\boldsymbol{x}$=0.7	4.191	3.666	3.883	3.542	3.983	2.730	4.307
$\boldsymbol{x}$=0.8	4.198	3.670	3.885	3.546	3.985	2.731	4.308
$\boldsymbol{x}$=0.9	4.205	3.675	3.886	3.550	3.988	2.732	4.310
RPBE	4.213	3.679	3.888	3.553	3.990	2.733	4.312
			SRP$\boldsymbol{x}$sol				
PBEsol	4.035	3.559	3.822	3.454	3.902	2.683	4.237
$\boldsymbol{x}$=0.1	4.051	3.570	3.828	3.464	3.910	2.688	4.244
$\boldsymbol{x}$=0.2	4.067	3.581	3.834	3.473	3.918	2.693	4.252
$\boldsymbol{x}$=0.3	4.083	3.593	3.841	3.482	3.927	2.698	4.260
$\boldsymbol{x}$=0.4	4.099	3.604	3.847	3.492	3.935	2.704	4.268
$\boldsymbol{x}$=0.5	4.117	3.616	3.854	3.502	3.944	2.709	4.275
$\boldsymbol{x}$=0.6	4.134	3.628	3.860	3.512	3.953	2.714	4.283
$\boldsymbol{x}$=0.7	4.152	3.641	3.867	3.522	3.962	2.719	4.290
$\boldsymbol{x}$=0.8	4.172	3.653	3.874	3.532	3.971	2.723	4.298
$\boldsymbol{x}$=0.9	4.192	3.666	3.881	3.543	3.980	2.728	4.305
RPBE	4.213	3.679	3.888	3.553	3.990	2.733	4.312

TABLE 5.A.2: Calculated barrier heights E_b computed with limiting forms of the mixed DFs are shown for the 16 systems present in the SBH16 database, as calculated for the PBE, the RPBE, the PBEsolc, the PBE-vdW1, the PBE-vdW2, and the PBEα-vdW1 DF with α=0.57. Also presented are the values of the charge excitation parameter ΔE_{CT}=WF-EA. The systems are arranged with the charge transfer parameter increasing from top to bottom.

System	E_b^{PBE}	E_b^{RPBE}	$E_b^{PBEsolc}$	$E_b^{PBE-vdW1}$	$E_b^{PBE-vdW2}$	$E_b^{PBE\alpha-vdW1}$	WF-EA
N_2+Ru(1010)	-0.096	0.469	-0.999	-0.023	0.247	-0.314	6.582
N_2+Ru(0001)	1.532	1.965	0.896	1.688	1.746	1.314	7.382
H_2+Ag(111)	1.132	1.457	0.643	1.442	1.569	1.275	7.685
H_2+Cu(110)	0.639	0.874	0.346	0.914	0.996	0.792	7.715
H_2+Cu(100)	0.584	0.905	0.095	0.894	1.024	0.731	7.885
H_2+Cu(111)	0.463	0.760	0.026	0.771	0.886	0.617	8.055
H_2+Ni(111)	0.026	0.170	-0.097	-0.006	0.085	-0.076	8.395
H_2+Ru(0001)	0.014	0.108	-0.050	-0.049	0.002	-0.096	8.555
H_2+Pt(111)	0.018	0.169	-0.103	-0.005	0.063	-0.079	9.065
CH_4+Ni(211)	0.675	0.973	0.349	0.603	0.777	0.448	10.72
CH_4+Ni(100)	0.912	1.259	0.491	0.843	1.020	0.664	10.92
CH_4+Ni(111)	1.010	1.349	0.594	0.962	1.156	0.785	10.99
CH_4+Ru(0001)	0.856	1.164	0.456	0.760	0.989	0.603	11.15
CH_4+Pt(211)	0.489	0.789	0.092	0.484	0.618	0.316	11.39
CH_4+Ir(111)	0.875	1.186	0.495	0.714	0.894	0.550	11.53
CH_4+Pt(111)	0.819	1.151	0.414	0.775	0.898	0.604	11.66

TABLE 5.A.3: Calculated barrier heights E_b computed with limiting forms of the mixed DFs are shown for the 16 systems present in the SBH16 database, as calculated for the the PBEα-vdW1 DF with α=0.57, the RPBE-vdW1 DF, the RPBE-vdW2 DF, and the PBEsol-vdW2 DF. Also presented are the values of the charge excitation parameter ΔE_{CT}=WF-EA. The systems are arranged with the charge transfer parameter increasing from top to bottom.

System	$E_b^{PBE\alpha-vdW2}$	$E_b^{RPBE-vdW1}$	$E_b^{RPBE-vdW2}$	$E_b^{PBEsol-vdW2}$	WF-EA
N_2+Ru(1010)	-0.044	0.525	0.801	-0.568	6.582
N_2+Ru(0001)	1.529	2.133	2.367	1.113	7.382
H_2+Ag(111)	1.403	1.758	1.885	1.114	7.685
H_2+Cu(110)	0.887	1.144	1.239	0.714	7.715
H_2+Cu(100)	0.859	1.205	1.332	0.564	7.885
H_2+Cu(111)	0.736	1.064	1.183	0.470	8.055
H_2+Ni(111)	-0.002	0.134	0.209	-0.045	8.395
H_2+Ru(0001)	-0.044	0.043	0.095	-0.052	8.555
H_2+Pt(111)	-0.012	0.145	0.211	-0.044	9.065
CH_4+Ni(211)	0.613	0.907	1.076	0.433	10.72
CH_4+Ni(100)	0.829	1.188	1.352	0.607	10.92
CH_4+Ni(111)	0.949	1.305	1.473	0.713	10.99
CH_4+Ru(0001)	0.775	1.063	1.235	0.565	11.15
CH_4+Pt(211)	0.474	0.790	0.939	0.232	11.39
CH_4+Ir(111)	0.730	1.030	1.210	0.501	11.53
CH_4+Pt(111)	0.726	1.107	1.262	0.529	11.66

TABLE 5.A.4: The optimal mixing coefficient $\boldsymbol{x}$ is shown for the mixed DFs SRP$\boldsymbol{x}$, SRP$\boldsymbol{x}$sol, SRP$\boldsymbol{x}$-vdW1, and SRP$\boldsymbol{x}$-vdW2. Also presented are the values of the charge excitation parameter ΔE_{CT}=WF-EA. The systems are arranged with the charge transfer parameter increasing from top to bottom.

System	WF-EA	SRP$\boldsymbol{x}$	SRP$\boldsymbol{x}$sol	SRP$\boldsymbol{x}$-vdW1	SRP$\boldsymbol{x}$-vdW2
N_2 + Ru(1010)	6.582	0.88	0.95	0.77	0.27
N_2 + Ru(0001)	7.382	0.71	0.88	0.34	0.01
H_2 + Ag(111)	7.685	-0.15	0.53	-1.14	-1.55
H_2 + Cu(110)	7.715	0.64	0.84	-0.55	-0.91
H_2 + Cu(100)	7.885	0.49	0.79	-0.49	-0.91
H_2 + Cu(111)	8.055	0.55	0.82	-0.49	-0.88
H_2 + Ni(111)	8.395	-0.02	0.45	0.21	-0.42
H_2 + Ru(0001)	8.555	-0.09	0.34	0.57	0.02
H_2 + Pt(111)	9.065	-0.17	0.34	-0.02	-0.48
CH_4 + Ni(211)	10.72	0.08	0.57	0.32	-0.24
CH_4 + Ni(100)	10.92	-0.44	0.34	-0.24	-0.76
CH_4 + Ni(111)	10.99	0.01	0.56	0.27	-0.26
CH_4 + Ru(0001)	11.15	-0.18	0.48	0.13	-0.44
CH_4 + Pt(211)	11.39	0.23	0.67	0.32	-0.14
CH_4 + Ir(111)	11.53	-0.12	0.49	0.39	-0.18
CH_4 + Pt(111)	11.66	0.00	0.54	0.24	-0.17

TABLE 5.A.5: The optimal mixing coefficient $\boldsymbol{x}$ is shown for the mixed DFs SRP$\boldsymbol{x}$sol-vdW2, SRP$\boldsymbol{x}$-vdW1-ext, and SRP$\boldsymbol{x}$-vdW2-ext. Also presented are the values of the charge excitation parameter ΔE_{CT}=WF-EA. The systems are arranged with the charge transfer parameter (see Table 5.A.4) increasing from top to bottom.

System	SRP$\boldsymbol{x}$sol-vdW2	SRP$\boldsymbol{x}$-vdW1-ext	SRP$\boldsymbol{x}$-vdW2-ext
N_2 + Ru(1010)	0.70	0.77	0.27
N_2 + Ru(0001)	0.66	0.34	0.01
H_2 + Ag(111)	-0.07	-0.90	-1.21
H_2 + Cu(110)	0.12	-0.46	-0.76
H_2 + Cu(100)	0.78	-0.42	-0.74
H_2 + Cu(111)	0.21	-0.42	-0.72
H_2 + Ni(111)	0.25	0.21	-0.31
H_2 + Ru(0001)	0.34	0.57	0.02
H_2 + Pt(111)	0.15	-0.06	-0.42
CH_4 + Ni(211)	0.42	0.32	-0.22
CH_4 + Ni(100)	0.19	-0.23	-0.60
CH_4 + Ni(111)	0.45	0.27	-0.21
CH_4 + Ru(0001)	0.67	0.13	-0.38
CH_4 + Pt(211)	0.50	0.32	-0.15
CH_4 + Ir(111)	0.53	0.39	-0.19
CH_4 + Pt(111)	0.55	0.24	-0.21

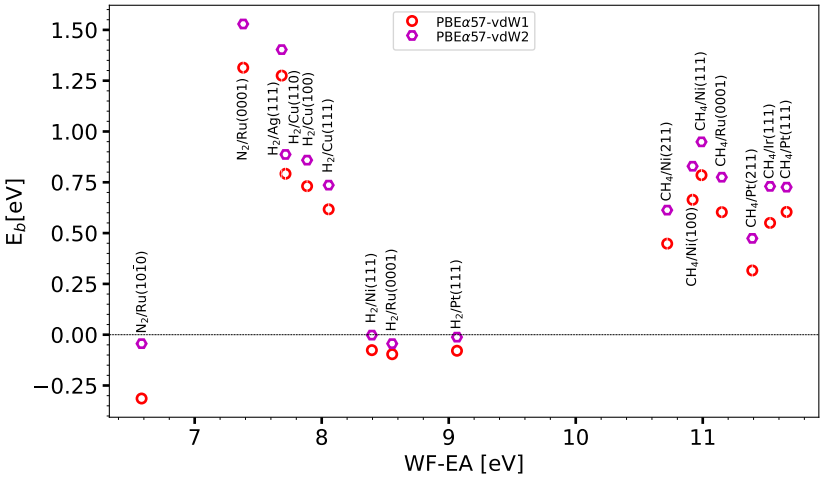

FIGURE 5.A.1: The barrier heights E_b computed with the PBEα-vdW1 and PBEα-vdW2 DFs with α=0.57 are shown as a function of the charge transfer parameter for the 16 systems present in the SBH16 database. These DFs may be viewed as the lower-limit expressions given by Eqs. 5.6b and 5.7b, respectively.

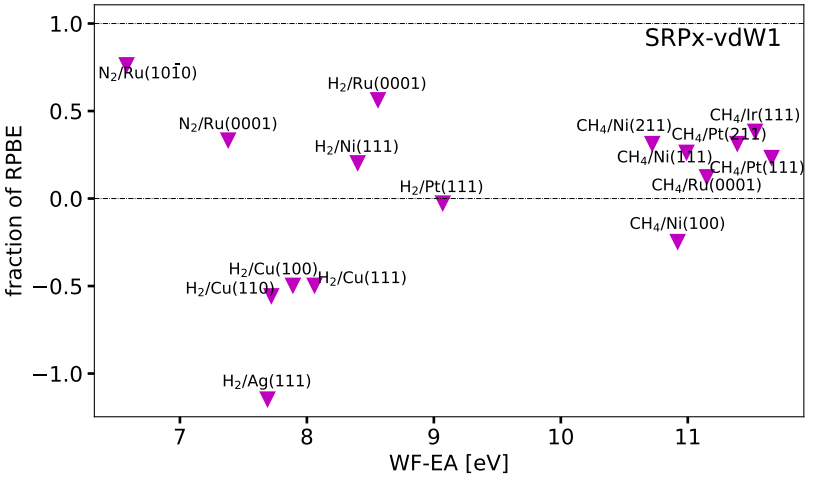

FIGURE 5.A.2: The optimum fraction of RPBE exchange $\boldsymbol{x}$ is shown as a function of ΔE_{CT} for the SRP$\boldsymbol{x}$-vdW1 DF (Eq.5.3). Values falling between the two horizontal dot-dashed black lines could be obtained by the interpolation procedure illustrated in Figure 5.5.

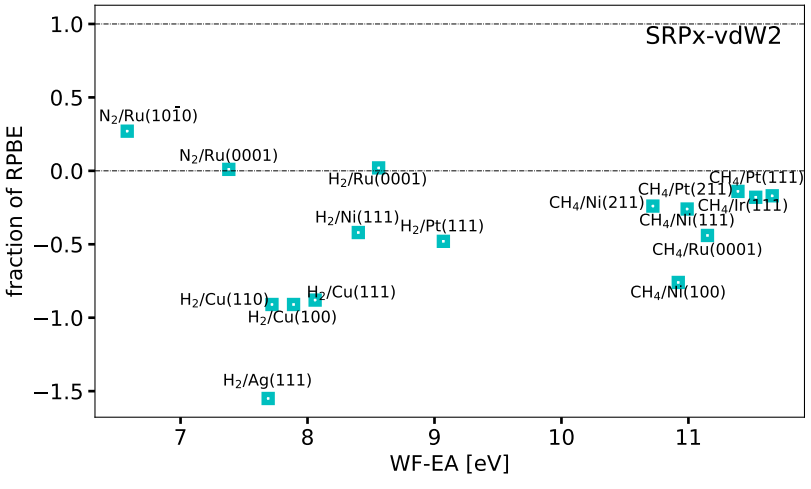

FIGURE 5.A.3: The optimum fraction of RPBE exchange $\boldsymbol{x}$ is shown as a function of ΔE_{CT} for the SRP$\boldsymbol{x}$-vdW2 DF (Eq.5.4). Values falling between the two horizontal dot-dashed black lines could be obtained by the interpolation procedure illustrated in Figure 5.5.

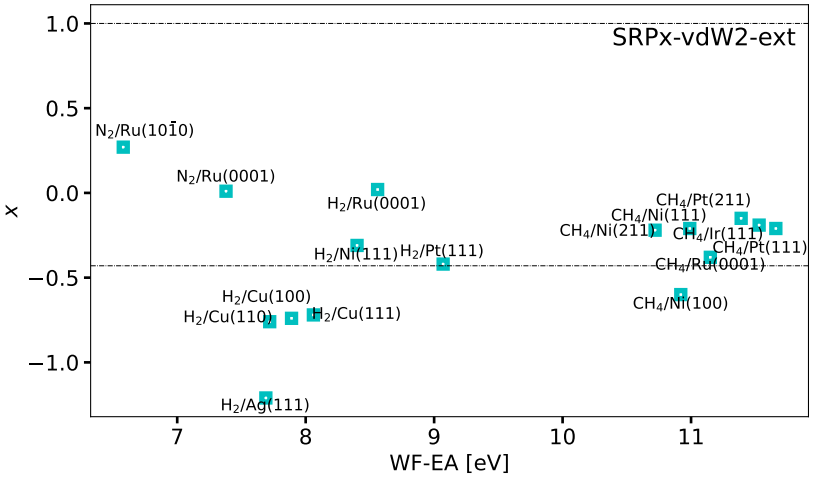

FIGURE 5.A.4: The optimum mixing parameter $\boldsymbol{x}$ is shown as a function of ΔE_{CT} for the SRP$\boldsymbol{x}$-vdW2-ext DF (Eq.5.7). Values falling between the two horizontal dot-dashed black lines could be obtained by the interpolation procedure illustrated in Figure 5.5.

References

(1) Wolcott, C. A.; Medford, A. J.; Studt, F.; Campbell, C. T. Degree of rate control approach to computational catalyst screening. *J. Catal.* **2015**, *330*, 197–207.

(2) Sabbe, M. K.; Reyniers, M.-F.; Reuter, K. First-principles kinetic modeling in heterogeneous catalysis: an industrial perspective on best-practice, gaps and needs. *Catal. Sci. Technol.* **2012**, *2*, 2010–2024.

(3) Ertl, G. Primary steps in catalytic synthesis of ammonia. *J. Vac. Sci. Technol., A: Vacuum, Surfaces, and Films* **1983**, *1*, 1247–1253.

(4) Honkala, K.; Hellman, A.; Remediakis, I.; Logadottir, A.; Carlsson, A.; Dahl, S.; Christensen, C. H.; Nørskov, J. K. Ammonia synthesis from first-principles calculations. *science* **2005**, *307*, 555–558.

(5) Chorkendorff, I.; Niemantsverdriet, J. W., *Concepts of modern catalysis and kinetics*; Wiley Online Library: 2003; Vol. 138.

(6) Kroes, G. J. Computational approaches to dissociative chemisorption on metals: towards chemical accuracy. *Phys. Chem. Chem. Phys.* **2021**, *23*, 8962–9048.

(7) **Tchakoua, T.**; Gerrits, N.; Smeets, E. W. F.; Kroes, G. J. SBH17: Benchmark Database of Barrier Heights for Dissociative Chemisorption on Transition Metal Surfaces. *J. Chem. Theory Comput.* **2023**, *19*, 245–270.

(8) Doblhoff-Dier, K.; Meyer, J.; Hoggan, P. E.; Kroes, G. J. Quantum Monte Carlo calculations on a benchmark molecule–metal surface reaction: H_2+ Cu (111). *J. Chem. Theory Comput.* **2017**, *13*, 3208–3219.

(9) Díaz, C.; Pijper, E.; Olsen, R. A.; Busnengo, H. F.; Auerbach, D. J.; Kroes, G. J. Chemically accurate simulation of a prototypical surface reaction: H_2 dissociation on Cu(111). *Science* **2009**, *326*, 832–834.

(10) Sementa, L.; Wijzenbroek, M.; Van Kolck, B. J.; Somers, M. F.; Al-Halabi, A.; Busnengo, H. F.; Olsen, R. A.; Kroes, G. J.; Rutkowski, M.; Thewes, C., et al. Reactive scattering of H_2 from Cu(100): comparison of dynamics calculations based on the specific reaction parameter approach to density functional theory with experiment. *J. Chem. Phys.* **2013**, *138*, 044708.

(11) Ghassemi, E. N.; Wijzenbroek, M.; Somers, M. F.; Kroes, G. J. Chemically accurate simulation of dissociative chemisorption of D_2 on Pt(111). *Chem. Phys. Lett.* **2017**, *683*, 329–335.

(12) Ghassemi, E. N.; Smeets, E. W. F.; Somers, M. F.; Kroes, G. J.; Groot, I. M.; Juurlink, L. B.; Füchsel, G. Transferability of the specific reaction parameter density functional for H_2 + Pt(111) to H_2 + Pt(211). *J. Phys. Chem. C* **2019**, *123*, 2973–2986.

(13) Wijzenbroek, M.; Kroes, G. J. The effect of the exchange-correlation functional on H_2 dissociation on Ru(0001). *J. Chem. Phys.* **2014**, *140*, 084702.

(14) **Tchakoua, T**; Smeets, E. W.; Somers, M.; Kroes, G. J. Toward a Specific Reaction Parameter Density Functional for H_2+ Ni(111): Comparison of Theory with Molecular Beam Sticking Experiments. *J. Phys. Chem. C* **2019**, *123*, 20420–20433.

(15) Smeets, E. W. F.; Kroes, G. J. Performance of Made Simple Meta-GGA Functionals with rVV10 Nonlocal Correlation for H_2+ Cu(111), D_2+Ag(111), H_2+Au(111), and D_2+Pt(111). *J. Phys. Chem. C* **2021**, *125*, 8993–9010.

(16) Shakouri, K.; Behler, J.; Meyer, J.; Kroes, G. J. Accurate neural network description of surface phonons in reactive gas-surface dynamics: N_2+ Ru(0001). *J. Phys. Chem. Lett.* **2017**, *8*, 2131–2136.

(17) Spiering, P.; Shakouri, K.; Behler, J.; Kroes, G. J.; Meyer, J. Orbital-dependent electronic friction significantly affects the description of reactive scattering of N_2 from Ru(0001). *J. Phys. Chem. Lett.* **2019**, *10*, 2957–2962.

(18) Nattino, F.; Migliorini, D.; Kroes, G. J.; Dombrowski, E.; High, E. A.; Killelea, D. R.; Utz, A. L. Chemically accurate simulation of a polyatomic molecule-metal surface reaction. *J. Phys. Chem. Lett.* **2016**, *7*, 2402–2406.

(19) Migliorini, D.; Chadwick, H.; Nattino, F.; Gutiérrez-González, A.; Dombrowski, E.; High, E. A.; Guo, H.; Utz, A. L.; Jackson, B.; Beck, R. D.; Kroes, G. J. Surface reaction barriometry: methane dissociation on flat and stepped transition-metal surfaces. *J. Phys. Chem. Lett.* **2017**, *8*, 4177–4182.

(20) Nattino, F.; Díaz, C.; Jackson, B.; Kroes, G. J. Effect of surface motion on the rotational quadrupole alignment parameter of D_2 reacting on Cu(111). *Phys. Rev. Lett.* **2012**, *108*, 236104.

(21) Dion, M.; Rydberg, H.; Schröder, E.; Langreth, D. C.; Lundqvist, B. I. Van der Waals Density Functional for General Geometries. *Phys. Rev. Lett.* **2004**, *92*, 246401.

(22) Lee, K.; Murray, É. D.; Kong, L.; Lundqvist, B. I.; Langreth, D. C. Higher-accuracy van der Waals density functional. *Phys. Rev. B* **2010**, *82*, 081101.

(23) Madsen, G. K. H. Functional form of the generalized gradient approximation for exchange: The PBEα functional. *Phys. Rev. B* **2007**, *75*, 195108.

(24) Smeets, E. W. F.; Voss, J.; Kroes, G. J. Specific Reaction Parameter Density Functional Based on the Meta-Generalized Gradient Approximation: Application to H_2+Cu(111) and H_2+Ag(111). *J. Phys. Chem. A* **2019**, *123*, 5395–5406.

(25) Gerrits, N.; Smeets, E. W.; Vuckovic, S.; Powell, A. D.; Doblhoff-Dier, K.; Kroes, G. J. Density functional theory for molecule–metal surface reactions: When does the generalized gradient approximation get it right, and what to do if it does not. *J. Phys. Chem. Lett.* **2020**, *11*, 10552–10560.

(26) Hammer, B.; Hansen, L. B.; Nørskov, J. K. Improved adsorption energetics within density-functional theory using revised Perdew-Burke-Ernzerhof functionals. *Phys. Rev. B* **1999**, *59*, 7413–7421.

(27) Nattino, F.; Migliorini, D.; Bonfanti, M.; Kroes, G. J. Methane dissociation on Pt(111): Searching for a specific reaction parameter density functional. *J. Chem. Phys.* **2016**, *144*, 044702.

(28) Perdew, J. P.; Chevary, J. A.; Vosko, S. H.; Jackson, K. A.; Pederson, M. R.; Singh, D. J.; Fiolhais, C. Atoms, molecules, solids, and surfaces: Applications of the generalized gradient approximation for exchange and correlation. *Phys. Rev. B: Condens. Matter Mater. Phys.* **1992**, *46*, 6671–6687.

(29) Perdew, J. P.; Burke, K.; Ernzerhof, M. Generalized Gradient Approximation Made Simple. *Phys. Rev. Lett.* **1996**, *77*, 3865–3868.

(30) Perdew, J. P.; Ruzsinszky, A.; Csonka, G. I.; Vydrov, O. A.; Scuseria, G. E.; Constantin, L. A.; Zhou, X.; Burke, K. Restoring the Density-Gradient Expansion for Exchange in Solids and Surfaces. *Phys. Rev. Lett.* **2008**, *100*, 136406.

(31) Wu, Z.; Cohen, R. E. More accurate generalized gradient approximation for solids. *Phys. Rev. B* **2006**, *73*, 235116.

(32) Kresse, G.; Hafner, J. Ab initio molecular dynamics for liquid metals. *Phys. Rev. B* **1993**, *47*, 558–561.

(33) Kresse, G.; Furthmüller, J. Efficiency of ab-initio total energy calculations for metals and semiconductors using a plane-wave basis set. *Comput. Mater. Sci.* **1996**, *6*, 15–50.

(34) Kresse, G.; Furthmüller, J. Efficient iterative schemes for ab initio total-energy calculations using a plane-wave basis set. *Phys. Rev. B* **1996**, *54*, 11169.

(35) Kresse, G.; Joubert, D. From ultrasoft pseudopotentials to the projector augmented-wave method. *Phys. Rev. B* **1999**, *59*, 1758–1775.

(36) Bahn, S. R.; Jacobsen, K. W. An object-oriented scripting interface to a legacy electronic structure code. *Comput. Sci. Eng.* **2002**, *4*, 56–66.

(37) Larsen, A. H.; Mortensen, J. J.; Blomqvist, J.; Castelli, I. E.; Christensen, R.; Dułak, M.; Friis, J.; Groves, M. N.; Hammer, B.; Hargus, C., et al. The atomic simulation environment—a Python library for working with atoms. *J. Phys.: Condens. Matter* **2017**, *29*, 273002.

(38) Román-Pérez, G.; Soler, J. M. Efficient implementation of a van der Waals density functional: application to double-wall carbon nanotubes. *Phys. Rev. Lett.* **2009**, *103*, 096102.

(39) Wellendorff, J.; Lundgaard, K. T.; Møgelhøj, A.; Petzold, V.; Landis, D. D.; Nørskov, J. K.; Bligaard, T.; Jacobsen, K. W. Density functionals for surface science: Exchange-correlation model development with Bayesian error estimation. *Phys. Rev. B* **2012**, *85*, 235149.

(40) Tran, F.; Stelzl, J.; Blaha, P. Rungs 1 to 4 of DFT Jacob's ladder: Extensive test on the lattice constant, bulk modulus, and cohesive energy of solids. *J. Chem. Phys.* **2016**, *144*, 204120.

(41) Schimka, L.; Harl, J.; Stroppa, A.; Grüneis, A.; Marsman, M.; Mittendorfer, F.; Kresse, G. Accurate surface and adsorption energies from many-body perturbation theory. *Nat. Mater.* **2010**, *9*, 741–744.

(42) Klimeš, J.; Bowler, D. R.; Michaelides, A. Van der Waals density functionals applied to solids. *Phys. Rev. B* **2011**, *83*, 195131.

(43) Hays, W. L., *Statistics. Holt–Saunders: Tokyo,* 1981.

(44) Shukla, V.; Jiao, Y.; Lee, J.-H.; Schröder, E.; Neaton, J. B.; Hyldgaard, P. Accurate Nonempirical Range-Separated Hybrid van der Waals Density Functional for Complex Molecular Problems, Solids, and Surfaces. *Phys. Rev. X* **2022**, *12*, 041003.

(45) Cooper, V. R. Van der Waals density functional: An appropriate exchange functional. *Phys. Rev. B* **2010**, *81*, 161104.

(46) Berland, K.; Hyldgaard, P. Exchange functional that tests the robustness of the plasmon description of the van der Waals density functional. *Phys. Rev. B* **2014**, *89*, 035412.

(47) Sun, J.; Ruzsinszky, A.; Perdew, J. P. Strongly constrained and appropriately normed semilocal density functional. *Phys. Rev. Lett.* **2015**, *115*, 036402.

(48) Krukau, A. V.; Vydrov, O. A.; Izmaylov, A. F.; Scuseria, G. E. Influence of the exchange screening parameter on the performance of screened hybrid functionals. *J. Chem. Phys.* **2006**, *125*, 224106.

(49) Shukla, V.; Jiao, Y.; Frostenson, C. M.; Hyldgaard, P. vdW-DF-ahcx: a range-separated van der Waals density functional hybrid. *J. Phys.: Condens. Matter* **2021**, *34*, 025902.

(50) Gerrits, N.; Geweke, J.; Smeets, E. W. F.; Voss, J.; Wodtke, A. M.; Kroes, G. J. Closing the Gap Between Experiment and Theory: Reactive Scattering of HCl from Au(111). *J. Phys. Chem. C* **2020**, *124*, 15944–15960.

(51) Behler, J.; Delley, B.; Lorenz, S.; Reuter, K.; Scheffler, M. Dissociation of O_2 at Al(111): The role of spin selection rules. *Phys. Rev. Lett.* **2005**, *94*, 036104.

(52) Haas, P.; Tran, F.; Blaha, P. Calculation of the lattice constant of solids with semilocal functionals. *Phys. Rev. B* **2009**, *79*, 085104.

(53) Arblaster, J. W. Crystallographic properties of ruthenium. *Platinum Met. Rev.* **2013**, *57*, 127–136.